Anisotropic superconductivity and magnetism in single-crystal $RbEuFe_4As_4$

M. P. Smylie,[1,2] K. Willa,[1] J.-K. Bao,[1] K. Ryan,[3] Z. Islam,[4] H. Claus,[1] Y. Simsek,[1] Z. Diao,[5,6] A. Rydh,[6] A. E. Koshelev,[1] W.-K. Kwok,[1] D. Y. Chung,[1] M. G. Kanatzidis,[1,7] and U. Welp[1]

[1]*Materials Science Division, Argonne National Laboratory, 9700 S. Cass Avenue, Argonne, Illinois 60439, USA*
[2]*Department of Physics, University of Notre Dame, Notre Dame, Indiana 46556, USA*
[3]*Department of Physics, University of Illinois at Urbana-Champaign, Urbana, Illinois 61801, USA*
[4]*Advanced Photon Source, Argonne National Laboratory, 9700 S. Cass Avenue, Lemont, Illinois 60439, USA*
[5]*Laboratory of Mathematics, Physics and Electrical Engineering, Halmstad University, SE-301 18 Halmstad, Sweden*
[6]*Department of Physics, Stockholm University, SE-106 91 Stockholm, Sweden*
[7]*Department of Chemistry, Northwestern University, Evanston, Illinois 60208, USA*

(Received 11 May 2018; published 5 September 2018)

We investigate the anisotropic superconducting and magnetic properties of single-crystal $RbEuFe_4As_4$ using magnetotransport and magnetization measurements. We determine a magnetic ordering temperature of the Eu moments of $T_m = 15$ K and a superconducting transition temperature of $T_c = 36.8$ K. The superconducting phase diagram is characterized by high upper critical field slopes of -70 and -42 kG/K for in-plane and out-of-plane fields, respectively, and a surprisingly low superconducting anisotropy of $\Gamma = 1.7$. Ginzburg-Landau parameters of $\kappa_c \sim 67$ and $\kappa_{ab} \sim 108$ indicate extreme type-II behavior. These superconducting properties are in line with those commonly seen in optimally doped Fe-based superconductors. In contrast, Eu magnetism is quasi-two dimensional (2D), as evidenced by highly anisotropic in-plane and out-of-plane exchange constants of 0.6 K and <0.04 K. A consequence of the quasi-2D nature of the Eu magnetism are strong magnetic fluctuation effects, a large suppression of the magnetic ordering temperature as compared to the Curie-Weiss temperature, and a kinklike anomaly in the specific heat devoid of any singularity. Magnetization curves reveal a clear magnetic easy-plane anisotropy with in-plane and out-of-plane saturation fields of 2 and 4 kG.

DOI: 10.1103/PhysRevB.98.104503

I. INTRODUCTION

Europium-containing Fe-based superconducting materials have emerged as model systems for the study of the interplay of magnetism and superconductivity [1,2]. They are the latest members of a family of superconductors in which superconductivity coexists with complete, magnetically ordered sublattices of local rare-earth (R) moments such as RRh_4B_4 [3], RMo_8S_8 [4,5], and the nickel borocarbides [6]. It is believed that in these compounds the magnetic moments and the superconducting electrons reside in different, essentially isolated sublattices, enabling the existence of superconductivity despite the high concentration of localized magnetic moments [6,7]. Among these, the europium-containing Fe-based superconducting materials stand out since they display simultaneously high magnetic ordering temperatures (15–20 K) and superconducting transition temperatures in excess of 30 K, implying sizable magnetic exchange interactions in the presence of strong superconducting pairing. Extensive work on $EuFe_2As_2$ (Eu-122)-derived compounds has shown that the nonsuperconducting parent compound undergoes a spin-density-wave (SDW) transition of the Fe magnetic moments near 195 K [8], and near $T_m \sim 19$ K a transition of the Eu moments into a type-A antiferromagnetic state in which ferromagnetically ordered Eu sheets are coupled antiferromagnetically along the c axis [9]. A similar magnetic structure has been found in the low-temperature phases of the Ho, Dy, and Pr borocarbides [10]. Upon the application of pressure [11,12] or doping with, among others, P [13,14], K [15–17], and Na [18,19], the SDW transition of Eu-122 is suppressed and superconductivity emerges at temperatures reaching up to $T_c \sim 30$ K. At the same time, the Eu moments in the case of $EuFe_2(As_{1-x}P_x)_2$ rotate from the ab plane close to the c axis [20]; however, T_c stays largely unaltered inside the superconducting dome. This apparent decoupling of the magnetic Eu sublattice from the superconducting electrons has been attributed to the multiorbital nature of the Fe-based superconductors in which magnetic exchange interactions and superconductivity are mediated by different groups of electrons and to the high upper critical fields that can withstand internal exchange and dipolar fields [2,21]. In addition, due to the crystal structure of $EuFe_2As_2$-based materials (see Fig. 1), partial cancellation of exchange and dipolar fields may arise at the location of the Fe atoms.

In this regard, the recent discovery of superconductivity in $RbEuFe_4As_4$ and $CsEuFe_4As_4$ [22–25] is significant, since in these materials the asymmetric environment of the Fe_2As_2 layers (see Fig. 1) precludes any cancellation effects. Nevertheless, T_c reaches 37 K, among the highest values of all 122-type materials, and exceeds the values of the nonmagnetic sister compounds $CaKFe_4As_4$ ($T_c = 35$ K) [26] and (La,Na)(Cs,Rb)Fe_4As_4 ($T_c \sim 25$ K) [27]. This is in contrast to the behavior of nickel borocarbides for which the incorporation of magnetic rare-earth ions leads to a clear suppression of T_c as compared to a nonmagnetic rare-earth ion [6]. $RbEuFe_4As_4$ and $CsEuFe_4As_4$ are intrinsically doped to 0.25 holes/Fe atom

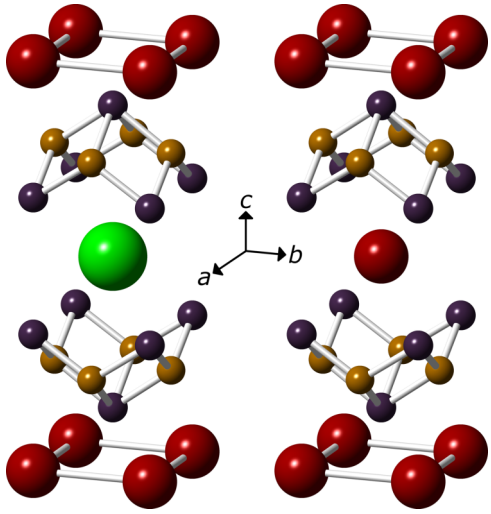

FIG. 1. (L) Crystal structure ($P4/mmm$) of $RbEuFe_4As_4$, with 2D sheets of Rb (green) and Eu (red) separated by Fe_2As_2 blocks. (R) Crystal structure ($I4/mmm$) of the parent compound $EuFe_2As_2$.

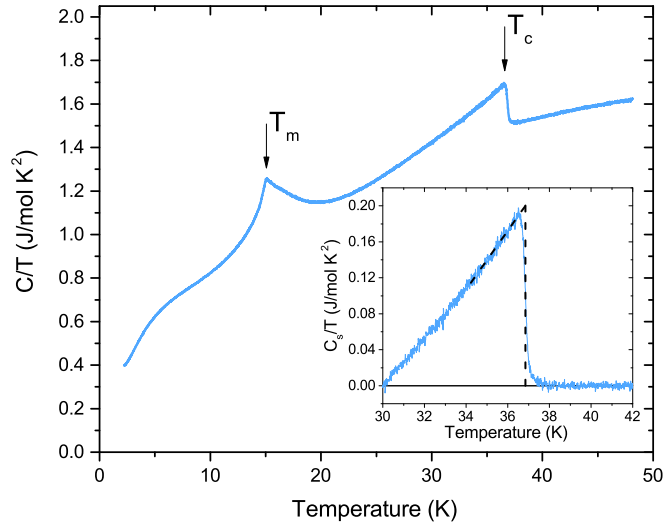

FIG. 2. Temperature dependence of C/T in zero-field specific heat of $RbEuFe_4As_4$. A clearly resolved kink at $T_m = 15$ K and a step at $T_c = 36.8$ K mark the magnetic and superconducting transitions, respectively. The inset shows the superconducting specific heat near the transition on enlarged scales. The lines illustrate the entropy-conserving construction.

such that in the stoichiometric material an electronic structure arises that closely corresponds to optimal doping in 122 materials. Furthermore, a recent study [28] revealed that upon Ni substitution on the Fe site, T_c is suppressed to zero and the SDW reemerges, while at the same time T_m is unchanged; similarly, Ca substitution on the Eu site [29] suppresses T_m without changing T_c, demonstrating the almost complete decoupling of the Eu sublattice from superconductivity.

Here we present a study of the anisotropic superconducting and magnetic properties of single-crystal $RbEuFe_4As_4$. Using magnetotransport and magnetization measurements, we determine a magnetic ordering temperature of the Eu moments of $T_m = 15$ K and a superconducting transition temperature of $T_c = 36.8$ K. The superconducting phase diagram is characterized by high upper critical field slopes of $dH_{c2}^{ab}/dT = -70$ kOe/K, $dH_{c2}^{c}/dT = -42$ kOe/K, and a surprisingly low superconducting anisotropy of $\Gamma = 1.7$. Ginzburg-Landau (GL) parameters of $\kappa_c \sim 67$ and $\kappa_{ab} \sim 108$ indicate extreme type-II behavior. These superconducting properties are in line with those commonly seen in optimally doped Fe-based superconductors. In contrast, Eu magnetism is highly anisotropic quasi-two dimensional (2D), as evidenced by anisotropic in-plane and out-of-plane exchange constants of 0.6 and <0.04 K, respectively. Consequences of the quasi-2D nature of the Eu magnetism are strong magnetic fluctuation effects, a negative magnetoresistance in high fields and at temperatures well above T_c, a large suppression of the magnetic ordering temperature as compared to the Curie-Weiss temperature, and a kinklike anomaly in the specific heat. Magnetization curves reveal a clear magnetic easy-plane anisotropy with in-plane and out-of-plane saturation fields of 2 and 4 kOe, respectively.

II. EXPERIMENTAL METHODS

High-quality single crystals of $RbEuFe_4As_4$ were grown using RbAs flux [30], yielding thin flat plates with sizes of up to 0.8 × 0.8 mm × 60 μm with the tetragonal c axis (001) perpendicular to the plate and the tetragonal (110) and $(1\bar{1}0)$ orientations parallel to the edges. For magnetotransport measurements, thin bars were cut from plates and gold wires were then attached with silver epoxy onto bar-shaped samples in a standard four-point configuration. For c-axis current measurements, sets of two contacts were placed on the top and bottom faces of the single crystal, roughly equally spaced. Magnetotransport measurements were performed in a 90-10-10 kG three-axis superconducting vector magnet, avoiding the need for mechanically rotating or remounting the samples, and magnetization measurements were performed on both zero field-cooling (ZFC) and field-cooling (FC) in a Quantum Design MPMS-7 system with samples attached to a quartz rod or quartz fiber. The specific heat of $RbEuFe_4As_4$ single crystals was measured using a membrane-based ac nanocalorimeter [31,32].

X-ray diffraction (XRD) and specific heat measurements revealed single-phase material without $EuFe_2As_2$ inclusions [30]. At room temperature, $RbEuFe_4As_4$ has a simple-tetragonal crystal structure ($P4/mmm$ space group) with one formula unit per unit cell and lattice constants of $a = 3.882$ Å and $c = 13.273$ Å (see Fig. 1). The large difference in ionic sizes of the Eu and Rb ions induces their segregation into sheets. The formal valence count reveals that $RbEuFe_4As_4$ is intrinsically doped to 0.25 holes/Fe atom. In contrast, the $EuFe_2As_2$ parent compound is at room temperature body-centered-tetragonal ($I4/mmm$ space group) containing two formula units per tetragonal unit cell.

III. RESULTS AND DISCUSSION

A. Specific heat

We evaluate the phase transitions occurring in single-crystal $RbEuFe_4As_4$ using zero-field specific heat measurements such as shown in Fig. 2 [30]. A clear kink in C/T at $T_m \sim 15$ K signals the magnetic transition, whereas a step in C/T at

$T_c \sim 36.8$ K is the signature of the superconducting transition. Our samples do not display an additional feature in the specific heat near 5 K that has been reported on polycrystalline samples [24,25] and was interpreted as signature of a transformation of a Fulde-Ferrell-Larkin-Ovchinnikov state into a spontaneous vortex state. We observe a fairly large step size of $\Delta C/T_c = 0.21$ J/mol K^2 at the superconducting transition as determined from the entropy-conserving construction (inset of Fig. 2). In single-band weak-coupling BCS theory, this step size corresponds to a large coefficient of the normal-state electronic specific heat of $\gamma_n = \Delta C/1.43T_c = 147$ mJ/mol K^2. Similar values have recently been reported for polycrystalline $RbEuFe_4As_4$ samples [24], as well as for crystals of the nonmagnetic sister compound $CaKFe_4As_4$ [26]. In single-band weak-coupling BCS theory, the normalized discontinuity of the slopes of the specific heat at T_c, $(T_c/\Delta C) * [\Delta(dC/dT)]|_{T_c}$, has a universal value of 2.64. Strong-coupling and multiband effects modify this value, as seen, for example, in Pb, for which a slope discontinuity of 4.6 has been reported [33] and the two-band superconductor MgB_2 for which a value of 3.35 can be deduced [34], respectively. From the data in Fig. 2 we obtain a very large value of $(T_c/\Delta C) * [\Delta(dC/dT)]|_{T_c} \sim 6.9$, which is similar to $Ba_{1-x}K_xFe_2As_2$ [35] and indicative of strong-coupling effects.

The kinklike feature at the magnetic transition does not display signatures commonly associated with a second-order transition, i.e., a step such as seen at the superconducting transition, or a singularity. This observation is in agreement with previous reports on polycrystalline $RbEuFe_4As_4$ [24] and $CsEuFe_4As_4$ [25] samples, where, following the Ehrenfest classification of phase transitions, it has been attributed to a third-order phase transition. As discussed in more detail below, such a shape of the specific heat anomaly can also arise from strong magnetic fluctuations and reduced dimensionality. The kink-shaped specific heat anomaly reported here is in contrast to the behavior seen in $EuFe_2As_2$, which shows a typical singular variation in the specific heat at the magnetic transition [8,13,36–38].

As shown in Fig. 1, an important difference between $RbEuFe_4As_4$ and $EuFe_2As_2$ is that in $RbEuFe_4As_4$ the distance between Eu layers is twice as large as in $EuFe_2As_2$, suggesting that reduced dimensionality and strong fluctuation effects lead to the marked difference in the specific heat signatures. In fact, due to the highly anisotropic exchange constants and the easy-plane magnetic anisotropy described in more detail below, the magnetism of Eu may be quasi-2D in $RbEuFe_4As_4$, exhibiting 2D-XY criticality and Berezinskii-Kosterlitz-Thouless behavior [39,40], while in $EuFe_2As_2$ it is more 3D-like, and more accurately described by a 3D-XY model accompanied by a singular specific heat as seen in experiment. Nevertheless, the measured kink in the specific heat (Fig. 2) is too sharp as compared to the predictions of the 2D-XY model [40]. However, Monte Carlo simulations of the 2D-to-3D crossover in the XY model clearly reveal the reemergence of the singularity in the specific heat with increasing 3D coupling [41], indicating quasi-2D behavior in the data of Fig. 2. Similarly, kinklike specific heat transitions arise in quasi-2D anisotropic Heisenberg models that depend on the coupling strength in the third direction [42]. A detailed examination of these phenomena is currently underway.

On decreasing temperature, the C/T data display a pronounced downward curvature. This feature, not seen on samples whose specific heat is dominated by the electronic and phonon contributions, has been reported for various high-spin systems [43,44]. It does not represent a phase transition, but qualitatively, it arises from the crossover from the quantum regime at low temperatures for which C approaches zero at zero temperature to the classical regime in which $C(T = 0)$ would be finite. This crossover is particularly sharp in high-S systems, since these follow classical behavior over most of the temperature range, and it is absent in $S = 1/2$ systems, as these are purely quantum mechanical.

B. Magnetic properties

We determine the magnetic state of $RbEuFe_4As_4$ using measurements of the field-cooled and zero-field-cooled temperature dependence, as well as the field dependence of the magnetization in fields applied along the ab planes and the c axis. In contrast to $EuFe_2As_2$, the magnetic transition of the Eu ions occurs deep in the superconducting state. Therefore, magnetization data at low temperatures, especially ZFC data and data for which $H//c$, contain contributions from superconducting vortices as well as from Eu moments.

The inset of Fig. 3(a) shows the temperature dependence of the magnetic susceptibility, $\chi = M/H$, measured in FC and ZFC conditions in several fields applied parallel to the in-plane (100) direction. The large diamagnetic signal observed near 37 K in the ZFC data marks the superconducting transition. The magnetic transition is seen as a clear cusp near $T_m = 15$ K, most notably in the ZFC data, whereas on field cooling, the susceptibility attains an almost temperature-independent value at the magnetic transition. In the case of $EuFe_2As_2$, similar magnetization behavior has been shown to arise from a transition into a type-A antiferromagnetic state. We note, however, that the actual magnetic ground state of $RbEuFe_4As_4$ is not known at present and that data such as shown in Fig. 3 are not able to establish it. For instance, $EuCo_2P_2$, which has the same crystal structure as Eu-122, displays magnetic behavior similar to that in Fig. 3, although a helical antiferromagnetic structure has been proposed for this material [45]. Furthermore, the data in Fig. 3 would also be consistent with a magnetic structure comprising a large net in-plane ferromagnetic component, as suggested by recent Mössbauer experiments on polycrystalline $RbEuFe_4As_4$ [46] and which could be expected on the basis of the doubling of the Eu-layer spacing [25] (see further discussion below).

Also included in the inset of Fig. 3(a) are data (green open circles) obtained following FC in 10 G after the sample was warmed on a ZFC run in 10 G up to 20 K, showing that it is not required to pass through the superconducting transition in order to induce the ferromagneticlike state. We note that, in general, this FM-like state is induced on field cooling in relatively low fields. The main panel in Fig. 3(a) displays the temperature dependence of the susceptibility measured after field cooling in a field of 1 kG applied along the three crystal axes. Under FC conditions for which the effects due to vortex pinning are small, we observe a large anisotropy in the low-temperature susceptibility with $\chi_{ab} \gg \chi_c$, revealing a pronounced easy-plane anisotropy of the Eu moments, similar to $EuFe_2As_2$, and

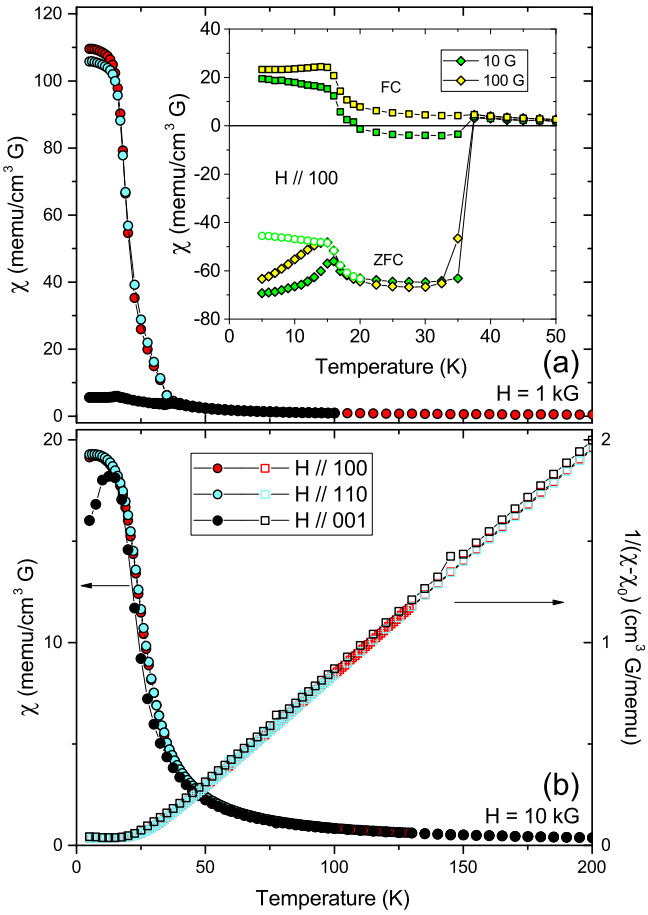

FIG. 3. Inset of panel (a): Temperature dependence of the susceptibility measured on FC (solid squares) and ZFC (solid diamonds) in 10 G (green symbols) and 100 G (yellow symbols) applied along the (100) direction. The open green circles are FC data in 10 G after warming to 20 K. Panels (a) and (b): Temperature dependence of the susceptibility after field cooling in a field of 1 and 10 kG along the (100), (110), and (001) directions. At temperatures above 50 K, the data are well described by the Curie-Weiss expression $\chi(T) = \chi_0 + C/(T - \Theta_C)$.

in agreement with the results of Mössbauer experiments [46]. The data also show that a possible in-plane magnetic anisotropy is comparatively very weak.

In higher fields [Fig. 3(b)], the difference between χ_{ab} and χ_c diminishes, indicating that magnetic saturation is approached. Below the ordering temperature, χ_c slightly decreases with decreasing temperature because the growing magnetic anisotropy pulls the Eu moments towards the planes. The data above 50 K are well described by a Curie-Weiss law $\chi(T) = \chi_0 + C/(T - \Theta_C)$, yielding for the (100), (110), and (001) directions values of Θ_C of 24.18 K, 23.81 K, and 22.32 K, respectively, and values for C of 7.476, 7.524, and 7.404 emu K/mol G, respectively. With $\mu_{eff} = 2.827 * C^{1/2}$, we find an effective moment of $\sim$7.75 μ_B per Eu ion. This value is close to the expected Eu^{2+} effective moment of $\mu_{eff} = g\mu_B\sqrt{S(S+1)} = 7.94\ \mu_B$/Eu (with $g = 2$ and $S = 7/2$), indicating that essentially all Eu ions are in the 2^+ state. The positive value of the Curie-Weiss temperature signals predominantly ferromagnetic interactions between the Eu moments consistent with a type-A antiferromagnetic structure. We observe a sizable reduction of the magnetic ordering temperature of $RbEuFe_4As_4$ ($T_m = 15$ K, $\Theta_C = 23$ K) as compared to Eu-122, for which a Curie-Weiss temperature of $\Theta_C \sim 21$ K and a magnetic ordering temperature $T_m \sim 19$ K have been determined [47]. We attribute this difference to the reduced dimensionality and strong magnetic fluctuations in $RbEuFe_4As_4$, while in Eu-122, which has the same layered spin arrangement albeit with half the distance of that in $RbEuFe_4As_4$, magnetic fluctuations have a relatively reduced effect consistent with the more conventional form of the specific heat anomaly as discussed above.

The values for χ_0 are 3.4×10^{-3} emu/mol G for the in-plane orientations and 3.1×10^{-3} emu/mol G for the c axis, representing anisotropic contributions from temperature-independent Pauli paramagnetism or van Vleck magnetism.

The insets of Figs. 4(a) and 4(b) show magnetization hysteresis loops measured at 5 K in H // (001) and H // (110). The superposition of a ferromagnetic-like signal and a hysteretic superconducting signal is clearly seen, especially for H // (001). This is expected due to the large sample cross section and high critical current density for this field orientation. Assuming that the superconducting hysteresis is symmetric around the equilibrium magnetization curve and that effects due to the hysteresis of the Eu magnetism are small (as is indicated by results on $EuFe_2As_2$ [47]), we extract the magnetization curve of the Eu sublattice as $(M_+ + M_-)/2$, where M_+ (M_-) is the magnetization measured in increasing (decreasing) applied field. The results, shown in the main panels of Figs. 4(a) and 4(b) for in-plane and out-of-plane field orientations, reveal ferromagnetic magnetization curves with a saturation magnetization of $\sim$320 emu/cm^3 at 5 K, corresponding to 6.7 μ_B/Eu, slightly less than the expected full moment of 7 μ_B/Eu. The comparison of magnetization curves measured along the three crystal axes [Fig. 4(c)] reveals a clear anisotropy in the approach to saturation, with the saturation fields of H // (110) and (100) being substantially smaller than for H // (001), while there is no discernible in-plane anisotropy. However, since the sample is platelike, such in-plane versus out-of-plane anisotropy may arise simply from demagnetization effects. The dashed lines in Fig. 4 indicate the corresponding demagnetization fields obtained by approximating the sample as an ellipsoid, demonstrating that the intrinsic saturation fields are indeed anisotropic with $H_{sat}^{ab} \sim 2.1$ kG and $H_{sat}^{c} \sim 4.2$ kG, consistent with easy-plane magnetic anisotropy. Eu^{2+} has a spin-only magnetic moment, and therefore, crystal electric field effects are not important in determining the single-ion magnetic anisotropy. In the case of Eu-122 it has been suggested [48] that dipolar interactions give rise to the easy-plane magnetic anisotropy.

In a model of a type-A antiferromagnet, the in-plane magnetization curves for which demagnetization effects are negligible allow for an estimate of the antiferromagnetic interlayer exchange constant J'. Neglecting a weak in-plane anisotropy, the magnetization curve for this orientation is given by $M/M_s = H/H_{af}$ [49], where $g\mu_B H_{af} = 2z'|J'|S$ defines the antiferromagnetic exchange field H_{af}, and $z' = 2$ is the number of nearest neighbors along the c axis yielding $J' \sim -0.04$ K. This value may be largely overestimated as $c \gg a$ (see Fig. 1), and the distance to the next-nearest neighbors

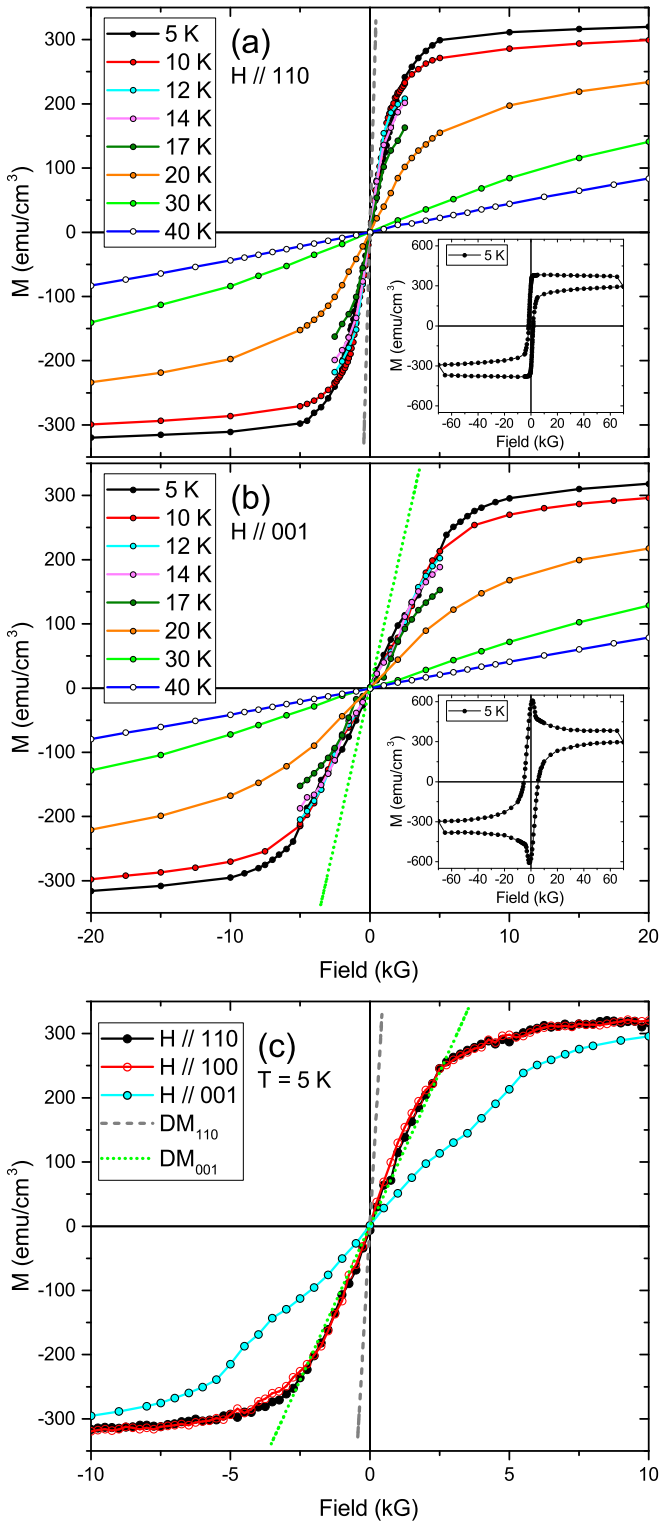

FIG. 4. Magnetization of the Eu sublattice vs applied field for (a) H // (110) and (b) H // (001) at various temperatures. The insets in (a) and (b) show the as-measured magnetization hysteresis loops. (c) A comparison of the magnetization at 5 K measured along the three crystal axes. The dashed lines represent the demagnetization fields due to the platelike sample geometry.

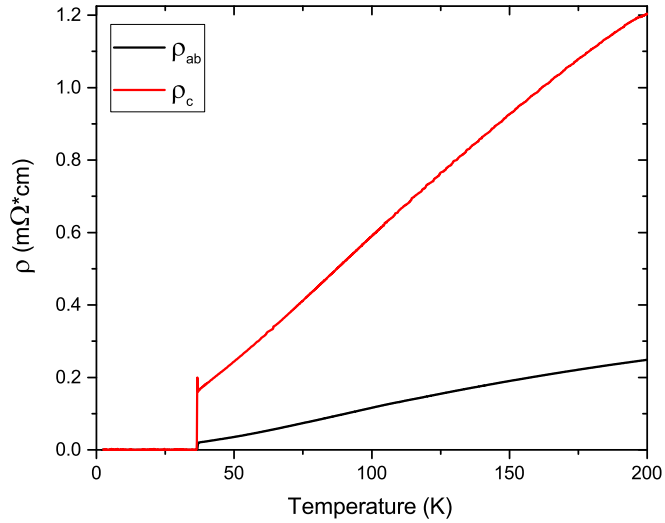

FIG. 5. Temperature dependence of the in-plane and out-of-plane resistivities of $RbEuFe_4As_4$. The anisotropy changes from ∼4 at 200 K to ∼8 near T_c.

along the c axis is only 4% larger than the nearest-neighbor distance and therefore an estimate with $z' \sim 10$ ($J' \sim -0.01$ K) would be more realistic. In comparison, the ferromagnetic in-plane exchange constant J, as estimated from the paramagnetic Curie-Weiss temperature $\Theta_C = 2[zJ + z'J']S(S+1)/3k_B$, is ∼0.6 K, underlining the quasi-2D nature of magnetism. Here, $z = 4$ is the number of in-plane nearest neighbors. We believe that these order-of-magnitude estimates of the anisotropic exchange interactions remain valid even if the magnetic structure is more complicated than type A, such as helical, for instance. As $RbEuFe_4As_4$ is metallic and the Eu-4f moments are well localized with the Eu ion situated ∼2 eV below the Fermi energy [8], the indirect Ruderman-Kittel-Kasuya-Yosida (RKKY) exchange interaction has been proposed as the mechanism of magnetic coupling [24]. While strong in-plane exchange interactions could also arise from superexchange, for instance, through the As site, exchange in the c direction and the onset of three-dimensional magnetic order will inevitably involve the predominantly Fe-3d states on two intervening superconducting FeAs layers. Orbital-selective magnetic and superconducting interactions may facilitate this coupling where superconductivity involves mainly d_{xz} and d_{yz} states [50,51], while the $d_{3z^2-r^2}$ orbital may transmit magnetic coupling along the c axis [52]. However, a recent study on polycrystalline Ni-for-Fe–substituted $RbEu(Fe_{1-x}Ni_x)_4As_4$ has shown that the magnetic ordering temperature is essentially independent of doping even as superconductivity is suppressed and a SDW on the Fe sites reemerges [28]. These results suggest that the RKKY interaction may not be the dominant interaction, and that the microscopic mechanisms underlying the simultaneous presence of sizable magnetic exchange and superconducting pairing interactions are not fully understood yet.

C. Resistivity

Figure 5 shows the temperature dependence of the in-plane (ρ_{ab}) and c-axis (ρ_c) electrical resistivities of $RbEuFe_4As_4$

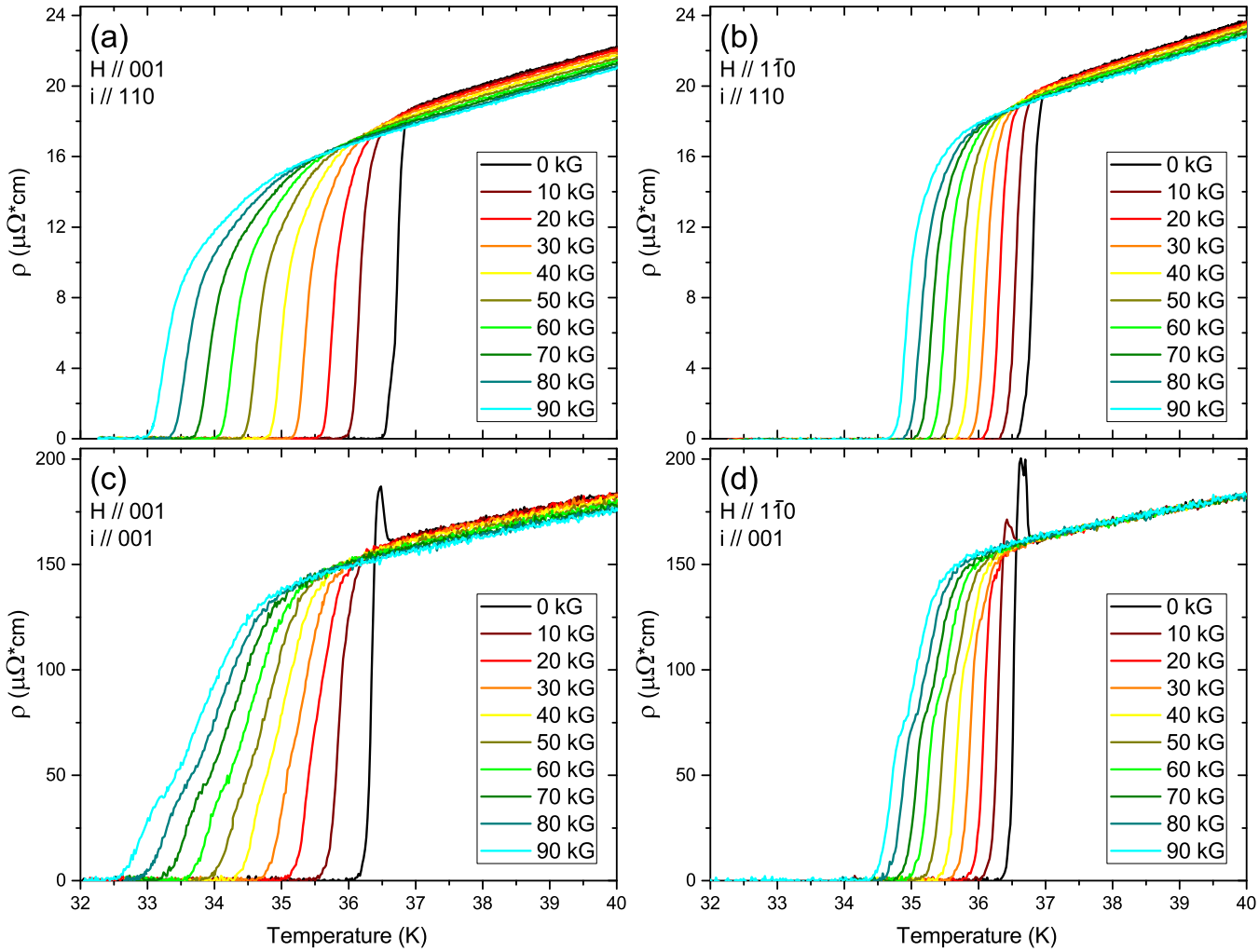

FIG. 6. Temperature and field dependence of the resistivity for various field and current configurations. (a, b) Current in-plane and field applied along the c axis and parallel to the ab planes, respectively. (c, d) c-axis current and field applied along the c axis and the ab planes.

measured with $i = 1$ mA. The residual resistivity $\rho_{ab}(0)$ is estimated at approximately 15 $\mu\Omega$ cm, indicating high-quality material. ρ_{ab} and ρ_c are metallic, a feature seen in other 1144-type and 122-type superconductors [26,53]. The resistivity anisotropy increases from ∼4 near 200 K to about 8 at T_c, similar to the behavior of nonmagnetic $CaKFe_4As_4$ [26]. Such temperature-dependent anisotropy could arise in a multiband system in which carriers in the different bands have different mobilities with different temperature dependences. In all samples studied, there is a sharp drop in the resistivity at the superconducting transition temperature of $T_c \sim 36.5$–36.8 K, with a transition width of 0.5 K or less. The sharp feature at the top of the c-axis resistive transition arises from nonideal contact geometry and the redistribution of the current flow at the superconducting transition [54]. Below T_c down to 1.6 K, we do not observe a reentrant resistive state associated with the onset of magnetic order of the Eu sublattice, unlike observed in other Eu-containing iron arsenides such as $Eu(Fe_{1-x}Ir_x)_2As_2$ and $EuFe_2As_2$ (under pressure) [55–57] or in several borocarbide superconductors [6,7]. Our finding is consistent with very weak coupling of Eu magnetism and superconductivity in $RbEuFe_4As_4$.

To study the superconducting anisotropy, resistivity measurements with applied magnetic field parallel to the (1$\bar{1}$0) (ab plane) or the (001) (c-axis) directions were performed (Fig. 6). Figures 6(a) and 6(b) show resistivity measurements up to 9 T with an ab-planar current of 1 mA, with the field parallel to c and parallel to ab, respectively, on the same single crystal of $RbEuFe_4As_4$. In both cases, the field was perpendicular to the current. A modest anisotropy, the rather large slopes of $H_{c2}(T)$, and negative normal-state magnetoresistance are all immediately noticeable. Figures 6(c) and 6(d) show resistivity measurements with 1 mA parallel to the c axis on a separate crystal, with the field parallel to c and ab, respectively. The results are qualitatively the same as for ab planar current.

The resistivity data corresponding to the normal state in Fig. 6 reveal a negative magnetoresistance (MR). Figure 7 shows measurements of the isothermal transverse MR, $\Delta\rho/\rho(H=0) = (\rho(H) - \rho(H=0))/\rho(H=0)$, for H // (001) and H // (1$\bar{1}$0) at various temperatures with current along (110). For H // (1$\bar{1}$0), the field and current were perpendicular. The MR was obtained by slowly sweeping the applied magnetic field from −9 to 9 T and by evaluating the symmetric part of the signal in order to eliminate

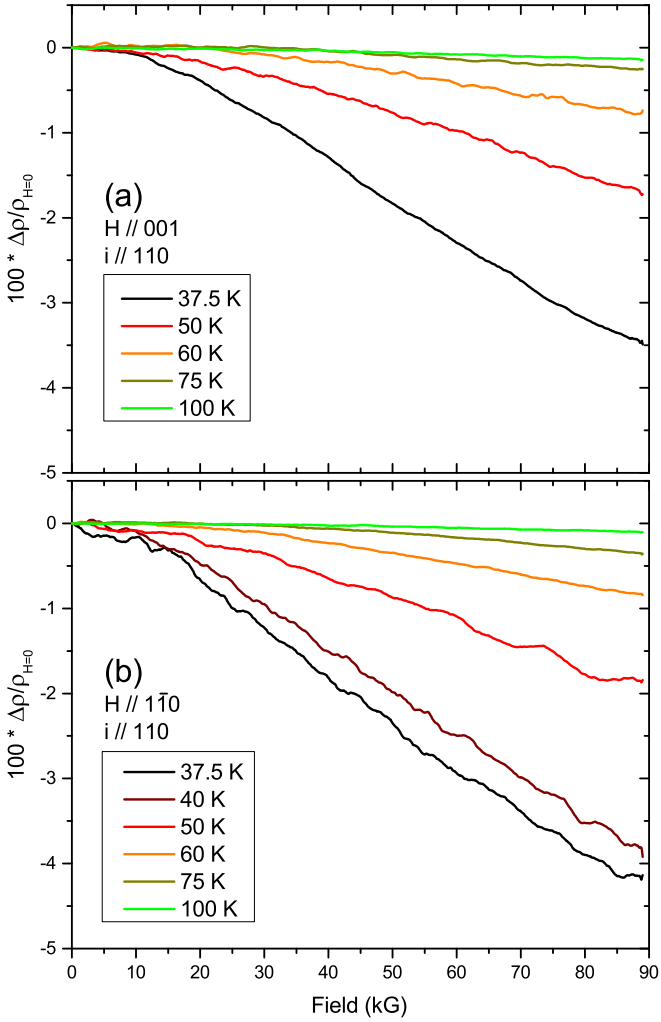

FIG. 7. Transverse magnetoresistance $\Delta\rho/\rho(H=0)$ at multiple fixed temperatures with i // (110) for (a) H // (001) and (b) H // (1$\bar{1}$0) in a single crystal of $RbEuFe_4As_4$.

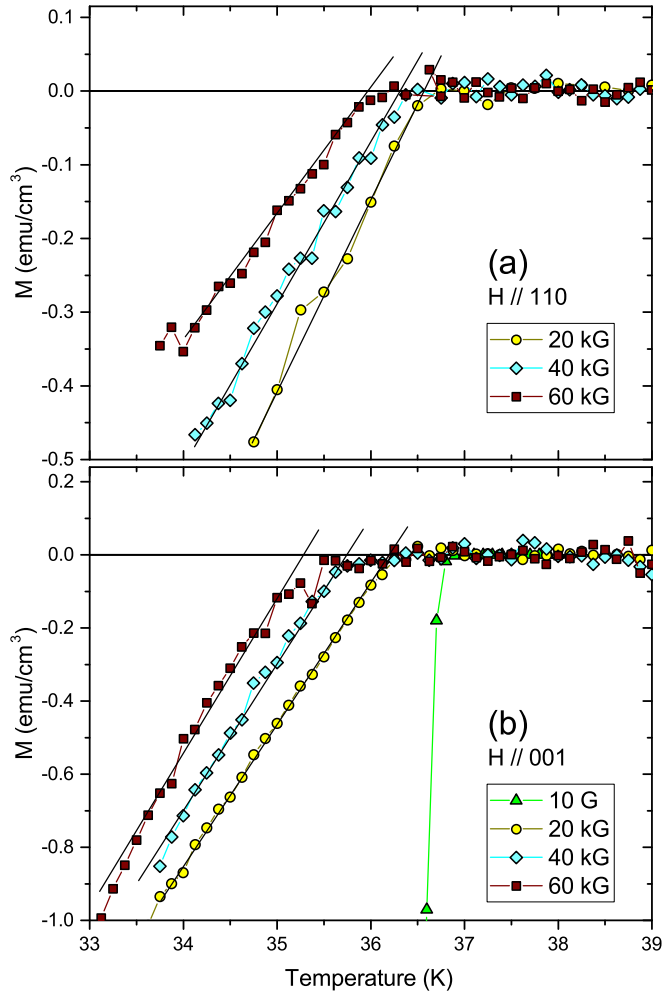

FIG. 8. Temperature dependence of the magnetization in various fields applied along the ab planes (a) and the c axis (b). The lines indicate the construction of $T_c(H)$.

spurious contributions from the Hall effect in nonideal contact geometries. Measurements at currents of 1 mA and 0.1 mA yielded the same results. We observe a clearly discernible negative transverse MR at temperatures above T_c, that is, in the paramagnetic state of the Eu ions. With increasing temperature the MR decreases rapidly. A negative MR has been observed previously in $EuFe_2As_2$ [47,58] in the magnetically ordered and paramagnetic states of the Eu sublattice, and has been attributed to the suppression of electron scattering by Eu spin fluctuations. An analysis based on the Yamada-Takada model [59] yielded a quantitative description of the effect [58]. The observation of a large magnetic contribution to the specific heat in high fields and at high temperatures [23,24] reveals sizable spin fluctuations at temperatures well above T_m and that a similar mechanism of negative MR may be active in $RbEuFe_4As_4$. The data at 37.5 K suggest a change in curvature of the MR at high fields, indicating the superposition of two effects, the negative MR at low fields due to suppression of spin scattering and the conventional positive MR due to the cyclotron motion of the carriers that grows as $(\mu H)^2$ where μ is the carrier mobility. As in the case of $EuFe_2As_2$, the negative MR is a small effect, of the order of a few percent.

D. Superconducting phase diagram

We determine the superconducting phase diagram of $RbEuFe_4As_4$ from the resistive transitions shown in Fig. 6 and from magnetization measurements in fields up to 60 kG (see Fig. 8). Here, a quadratic polynomial in $1/T$ has been fitted between 37 and 40 K and subtracted from the magnetization data such as those shown in Fig. 3(b) to reveal the superconducting signature. The anisotropic shift of the superconducting transition in applied fields is clearly seen. We observe that the 90%-ρ_n criterion and the magnetic determination yield consistent measures of $T_c(H)$. The resulting phase boundaries are shown in Fig. 9. We find enormous upper critical fields H_{c2} and remarkably low superconducting anisotropies Γ, in line with the behavior generally seen for Fe-based superconductors. We obtain $dH_{c2}^{ab}/dT = -70$ kG/K, $dH_{c2}^{c}/dT = -42$ kG/K, and $\Gamma = 1.7$ (not including the upward curvature near T_c, which is not apparent in the magnetization data). The value for the anisotropy is lower than expected on the basis of the

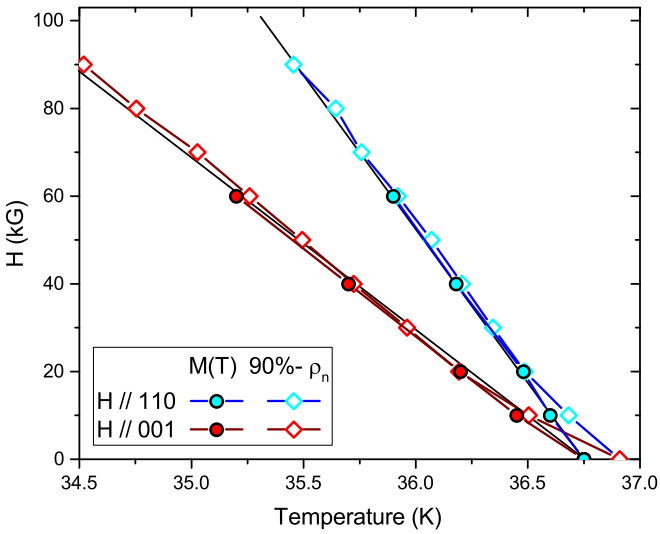

FIG. 9. The upper critical field of $RbEuFe_4As_4$ as determined from magnetization (closed circles) and magnetotransport (open diamonds) measurements.

resistivity anisotropy and a single-band Drude model for which $\Gamma \sim \sqrt{\rho_c/\rho_{ab}}$ suggestive of multiband effects and potential gap anisotropy.

Results obtained on the nonmagnetic sister compound $CaKFe_4As_4$ [26,60] suggest that $RbEuFe_4As_4$ is a multiband superconductor; however, as neither the inter- and intraband pairing constants nor the details of the Fermi surface are known, we present an approximate discussion of the upper critical field using a single-band formalism. Using the GL relationship $H_{c2}(0) = -(dH_{c2}/dT)|_{T_c} * T_c$, we estimate zero-temperature values of $H^{ab}_{c2}(0) \sim 2500$ kG and $H^{c}_{c2}(0) \sim 1600$ kG, very large but comparable to other Fe-based superconductors [61,62]. These estimates exceed the BCS paramagnetic limit $H_p(\mathrm{kG}) = (1+\lambda) * 18.4T_c(\mathrm{K})$, where λ is the electron-boson coupling constant [63], even when including strong-coupling effects, indicating that at low temperatures deviations from the GL extrapolation will occur. Nevertheless, the in-plane and out-of-plane GL coherence lengths ξ_{ab} and ξ_c may be estimated using the single-band Ginzburg-Landau relations $H^{c}_{c2}(0) = \Phi_0/2\pi\xi^2_{ab}(0)$ and $H^{ab}_{c2}(0) = \Phi_0/[2\pi\xi_{ab}(0)\xi_c(0)]$, yielding $\xi_c(0) = 0.92$ nm and $\xi_{ab} = 1.4$ nm. The estimate for $\xi_c(0)$ is slightly smaller than the c-axis lattice constant, making the low value of the anisotropy all the more surprising.

With the help of the Rutgers relation a connection between the jump in the specific heat and the superconducting phase boundaries can be established: $\Delta C/T_c = (dH^i_{c2}/dT|_{T_c})^2/8\pi\kappa_i^2$. With $\Delta C/T_c = 0.21$ J/mol K^2 and the upper critical field slopes from Fig. 9 we obtain the GL parameters $\kappa_c = \lambda_{ab}/\xi_{ab} \sim 67$ and $\kappa_{ab} = \sqrt{\lambda_{ab}\lambda_c}/\sqrt{\xi_{ab}\xi_c} \sim 108$, consistent with determinations based on the slopes of the $M(T)$ curves shown in Fig. 8. Thus, $RbEuFe_4As_4$ is in the extreme type-II limit, as is commonly observed for the Fe-based superconductors.

These materials parameters allow one to estimate the Ginzburg number G_i, which describes the importance of superconducting thermal fluctuations, as $G_i = [8\pi^2 k_B \Gamma T_c \kappa_c^2 \xi_{ab}/\phi_0^2]^2/2 \approx 7 \times 10^{-5}$. This relatively low value is of the same order of magnitude as seen in other 122 and 1144 Fe-based superconductors [26,64] and is consistent with the almost complete absence of fluctuation effects at the superconducting transition (see inset of Fig. 2). In contrast, G_i is significantly larger in the 1111 compounds, $G_i \sim 10^{-3} - 10^{-2}$ [65–67], the principal difference being the much larger anisotropy of the 1111 materials.

IV. CONCLUSION

In summary, among the superconductors containing ordered sublattices of rare-earth magnetic moments $RbEuFe_4As_4$ attains a special place due to its high magnetic and superconducting transition temperatures. Orbital-selective superconducting pairing and magnetic exchange may offer a framework for the coexistence of strong superconducting pairing and sizable magnetic interactions in this layered material, even though the underlying microscopic mechanisms have not been clarified yet. The high value of T_c, exceeding that of the nonmagnetic sister compound $CaKFe_4As_4$ [26], doping studies [28,29], and the surprisingly low value of the superconducting anisotropy, $\Gamma \sim 1.7$, indicate that both interaction channels are largely decoupled. In contrast to superconductivity, Eu magnetism is highly anisotropic quasi-2D, reflecting the large separation between the Eu layers. In a model of a type-A antiferromagnetic structure, we estimate in-plane and out-of-plane exchange constants of 0.6 K and less than 0.04 K, respectively. This reduced dimensionality induces strong magnetic fluctuations, a sizable suppression of the magnetic ordering temperature below the paramagnetic Curie-Weiss temperature, and a kinklike specific heat anomaly devoid of any singular behavior. These features distinguish $RbEuFe_4As_4$ from the parent compound $EuFe_2As_2$ in which the distance between Eu layers is half and magnetism is more 3D-like. Magnetization curves reveal a clear magnetic easy-plane anisotropy of $RbEuFe_4As_4$ with in-plane and out-of-plane saturation fields of 2 and 4 kG, respectively. Further measurements will be necessary to determine the true magnetic ground state of $RbEuFe_4As_4$.

ACKNOWLEDGMENTS

This work was supported by the U.S. Department of Energy, Office of Science, Basic Energy Sciences, Materials Sciences and Engineering Division. This research used resources of the Advanced Photon Source, a U.S. Department of Energy (DOE) Office of Science User Facility operated for the DOE Office of Science by Argonne National Laboratory under Contract No. DE-AC02-06CH11357. M.P.S. thanks ND Energy for supporting his research and professional development through the NDEnergy Postdoctoral Fellowship Program. K.W. acknowledges support through an Early Postdoc Mobility Fellowship of the Swiss National Science Foundation. Z.D. acknowledges support from the Swedish Research Council (VR) under Grant No. 2015-00585, cofunded by Marie Skłodowska-Curie Actions (Project No. INCA 600398). A.R. acknowledges support from the Swedish Research Council (VR) under Grant No. 2016-04516. The authors thank Roland Willa for helpful discussions.

[1] S. Zapf and M. Dressel, Rep. Prog. Phys. **80**, 016501 (2017).

[2] G.-H. Cao, W.-H. Jiao, Y.-K. Luo, Z. Ren, S. Jiang, and Z.-A. Xu, J. Phys.: Conf. Ser. **391**, 012123 (2012).

[3] *Superconductivity in Ternary Compounds II, Superconductivity and Magnetism*, edited by M. B. Maple and Ø. Fischer (Springer, New York, 1982).

[4] Ø. Fischer and M. B. Maple, *Ferromagnetic Materials* (Elsevier, New York, 1990), Vol. 5.

[5] P. C. Canfield, P. L. Gammel, and D. J. Bishop, Phys. Today **51**(10), 40 (1998).

[6] K.-H. Müller and V. N. Narozhnyi, Rep. Prog. Phys. **64**, 943 (2001).

[7] H. Eisaki, H. Takagi, R. J. Cava, B. Batlogg, J. J. Krajewski, W. F. Peck, K. Mizuhashi, J. O. Lee, and S. Uchida, Phys. Rev. B **50**, 647 (1994).

[8] H. S. Jeevan, Z. Hossain, D. Kasinathan, H. Rosner, C. Geibel, and P. Gegenwart, Phys. Rev. B **78**, 052502 (2008).

[9] Y. Xiao, Y. Su, M. Meven, R. Mittal, C. M. N. Kumar, T. Chatterji, S. Price, J. Persson, N. Kumar, S. K. Dhar *et al.*, Phys. Rev. B **80**, 174424 (2009).

[10] J. W. Lynn, S. Skanthakumar, Q. Huang, S. K. Sinha, Z. Hossain, L. C. Gupta, R. Nagarajan, and C. Godart, Phys. Rev. B **55**, 6584 (1997).

[11] C. F. Miclea, M. Nicklas, H. S. Jeevan, D. Kasinathan, Z. Hossain, H. Rosner, P. Gegenwart, C. Geibel, and F. Steglich, Phys. Rev. B **79**, 212509 (2009).

[12] K. Matsubayashi, K. Munakata, M. Isobe, N. Katayama, K. Ohgushi, Y. Ueda, N. Kawamura, M. Mizumaki, N. Ishimatsu, M. Hedo *et al.*, Phys. Rev. B **84**, 024502 (2011).

[13] Z. Ren, Q. Tao, S. Jiang, C. Feng, C. Wang, J. Dai, G. Cao, and Z. Xu, Phys. Rev. Lett. **102**, 137002 (2009).

[14] H. S. Jeevan, D. Kasinathan, H. Rosner, and P. Gegenwart, Phys. Rev. B **83**, 054511 (2011).

[15] H. S. Jeevan, Z. Hossain, D. Kasinathan, H. Rosner, C. Geibel, and P. Gegenwart, Phys. Rev. B **78**, 092406 (2008).

[16] J. Maiwald, H. S. Jeevan, and P. Gegenwart, Phys. Rev. B **85**, 024511 (2012).

[17] Anupam, P. L. Paulose, S. Ramakrishnan, and Z. Hossain, J. Phys.: Condens. Matter **23**, 455702 (2011).

[18] Y. Qi, Z. Gao, L. Wang, D. Wang, X. Zhang, and Y. Ma, New J. Phys. **10**, 123003 (2008).

[19] Y. Qi, L. Wang, Z. Gao, X. Zhang, D. Wang, C. Yao, C. Wang, C. Wang, and Y. Ma, New J. Phys. **14**, 033011 (2012).

[20] S. Nandi, W. T. Jin, Y. Xiao, Y. Su, S. Price, W. Schmidt, K. Schmalzl, T. Chatterji, H. S. Jeevan, P. Gegenwart *et al.*, Phys. Rev. B **90**, 094407 (2014).

[21] G. Cao, S. Xu, Z. Ren, S. Jiang, C. Feng, and Z. Xu, J. Phys.: Condens. Matter **23**, 464204 (2011).

[22] K. Kawashima, T. Kinjo, T. Nishio, S. Ishida, H. Fujihisa, Y. Gotoh, K. Kihou, H. Eisaki, Y. Yoshida, and A. Iyo, J. Phys. Soc. Jpn. **85**, 064710 (2016).

[23] A. Iyo, K. Kawashima, T. Kinjo, T. Nishio, S. Ishida, H. Fujihisa, Y. Gotoh, K. Kihou, H. Eisaki, and Y. Yoshida, J. Am. Chem. Soc. **138**, 3410 (2016).

[24] Y. Liu, Y.-B. Liu, Z.-T. Tang, H. Jiang, Z.-C. Wang, A. Ablimit, W.-H. Jiao, Q. Tao, C.-M. Feng, Z.-A. Xu *et al.*, Phys. Rev. B **93**, 214503 (2016).

[25] Y. Liu, Y.-B. Liu, Q. Chen, Z.-T. Tang, W.-H. Jiao, Q. Tao, Z.-A. Xu, and G.-H. Cao, Sci. Bull. **61**, 1213 (2016).

[26] W. R. Meier, T. Kong, U. S. Kaluarachchi, V. Taufour, N. H. Jo, G. Drachuck, A. E. Böhmer, S. M. Saunders, A. Sapkota, A. Kreyssig *et al.*, Phys. Rev. B **94**, 064501 (2016).

[27] K. Kawashima, S. Ishida, H. Fujihisa, Y. Gotoh, K. Kihou, Y. Yoshida, H. Eisaki, H. Ogino, and A. Iyo, J. Phys. Chem. Lett. **9**, 868 (2018).

[28] Y. Liu, Y.-B. Liu, Y.-L. Yu, Q. Tao, C.-M. Feng, and G.-H. Cao, Phys. Rev. B **96**, 224510 (2017).

[29] K. Kawashima, S. Ishida, K. Oka, H. Kito, N. Takeshita, H. Fujihisa, Y. Gotoh, K. Kihou, H. Eisaki, Y. Yoshida *et al.*, J. Phys.: Conf. Ser. **969**, 012027 (2018).

[30] J.-K. Bao, K. Willa, M. P. Smylie, H. Chen, U. Welp, D. Y. Chung, and M. G. Kanatzidis, Cryst. Growth Des. **18**, 3517 (2018).

[31] S. Tagliati, V. M. Krasnov, and A. Rydh, Rev. Sci. Instrum. **83**, 055107 (2012).

[32] K. Willa, Z. Diao, D. Campanini, U. Welp, R. Divan, M. Hudl, Z. Islam, W.-K. Kwok, and A. Rydh, Rev. Sci. Instrum. **88**, 125108 (2017).

[33] J. P. Carbotte, Rev. Mod. Phys. **62**, 1027 (1990).

[34] F. Bouquet, R. A. Fisher, N. E. Phillips, D. G. Hinks, and J. D. Jorgensen, Phys. Rev. Lett. **87**, 047001 (2001).

[35] U. Welp, R. Xie, A. E. Koshelev, W. K. Kwok, H. Q. Luo, Z. S. Wang, G. Mu, and H. H. Wen, Phys. Rev. B **79**, 094505 (2009).

[36] Z. Ren, Z. Zhu, S. Jiang, X. Xu, Q. Tao, C. Wang, C. Feng, G. Cao, and Z. Xu, Phys. Rev. B **78**, 052501 (2008).

[37] U. B. Paramanik, P. L. Paulose, S. Ramakrishnan, A. K. Nigam, C. Geibel, and Z. Hossain, Supercond. Sci. Technol. **27**, 075012 (2014).

[38] A. Oleaga, A. Salazar, A. Thamizhavel, and S. Dhar, J. Alloys Compd. **617**, 534 (2014).

[39] J. Tobochnik and G. V. Chester, Phys. Rev. B **20**, 3761 (1979).

[40] R. Gupta and C. F. Baillie, Phys. Rev. B **45**, 2883 (1992).

[41] W. Janke and T. Matsui, Phys. Rev. B **42**, 10673 (1990).

[42] P. Sengupta, A. W. Sandvik, and R. R. P. Singh, Phys. Rev. B **68**, 094423 (2003).

[43] D. C. Johnston, R. J. McQueeney, B. Lake, A. Honecker, M. E. Zhitomirsky, R. Nath, Y. Furukawa, V. P. Antropov, and Y. Singh, Phys. Rev. B **84**, 094445 (2011).

[44] M. Bouvier, P. Lethuillier, and D. Schmitt, Phys. Rev. B **43**, 13137 (1991).

[45] N. S. Sangeetha, E. Cuervo-Reyes, A. Pandey, and D. C. Johnston, Phys. Rev. B **94**, 014422 (2016).

[46] M. A. Albedah, F. Nejadsattari, Z. M. Stadnik, Y. Liu, and G.-H. Cao, Phys. Rev. B **97**, 144426 (2018).

[47] S. Jiang, Y. Luo, Z. Ren, Z. Zhu, C. Wang, X. Xu, Q. Tao, G. Cao, and Z. Xu, New J. Phys. **11**, 025007 (2009).

[48] Y. Xiao, Y. Su, W. Schmidt, K. Schmalzl, C. M. N. Kumar, S. Price, T. Chatterji, R. Mittal, L. J. Chang, S. Nandi *et al.*, Phys. Rev. B **81**, 220406 (2010).

[49] K. H. J. Buschow and F. R. de Boer, *Physics of Magnetism and Magnetic Materials*, 1st ed. (Springer New York, 2003).

[50] P. O. Sprau, A. Kostin, A. Kreisel, A. E. Böhmer, V. Taufour, P. C. Canfield, S. Mukherjee, P. J. Hirschfeld, B. M. Andersen, and J. C. S. Davis, Science **357**, 75 (2017).

[51] S. Raghu, X.-L. Qi, C.-X. Liu, D. J. Scalapino, and S.-C. Zhang, Phys. Rev. B **77**, 220503 (2008).

[52] Z. Ren, X. Lin, Q. Tao, S. Jiang, Z. Zhu, C. Wang, G. Cao, and Z. Xu, Phys. Rev. B **79**, 094426 (2009).

[53] M. A. Tanatar, N. Ni, G. D. Samolyuk, S. L. Bud'ko, P. C. Canfield, and R. Prozorov, Phys. Rev. B **79**, 134528 (2009).
[54] R. Vaglio, C. Attanasio, L. Maritato, and A. Ruosi, Phys. Rev. B **47**, 15302 (1993).
[55] N. Kurita, M. Kimata, K. Kodama, A. Harada, M. Tomita, H. S. Suzuki, T. Matsumoto, K. Murata, S. Uji, and T. Terashima, Phys. Rev. B **83**, 214513 (2011).
[56] U. B. Paramanik, D. Das, R. Prasad, and Z. Hossain, J. Phys.: Condens. Matter **25**, 265701 (2013).
[57] W.-H. Jiao, Q. Tao, J.-K. Bao, Y.-L. Sun, C.-M. Feng, Z.-A. Xu, I. Nowik, I. Felner, and G.-H. Cao, Europhys. Lett. **95**, 67007 (2011).
[58] T. Terashima, N. Kurita, A. Kikkawa, H. S. Suzuki, T. Matsumoto, K. Murata, and S. Uji, J. Phys. Soc. Jpn. **79**, 103706 (2010).
[59] H. Yamada and S. Takada, J. Phys. Soc. Jpn. **34**, 51 (1973).
[60] S. Teknowijoyo, K. Cho, M. Konczykowski, E. I. Timmons, M. A. Tanatar, W. R. Meier, M. Xu, S. L. Bud'ko, P. C. Canfield, and R. Prozorov, Phys. Rev. B **97**, 140508 (2018).
[61] H. Q. Yuan, J. Singleton, F. F. Balakirev, S. A. Baily, G. F. Chen, J. L. Luo, and N. L. Wang, Nature (London) **457**, 565 (2009).
[62] A. Gurevich, Nat. Mater. **10**, 255 (2011).
[63] M. Schossmann and J. P. Carbotte, Phys. Rev. B **39**, 4210 (1989).
[64] C. Chaparro, L. Fang, H. Claus, A. Rydh, G. W. Crabtree, V. Stanev, W. K. Kwok, and U. Welp, Phys. Rev. B **85**, 184525 (2012).
[65] U. Welp, R. Xie, A. E. Koshelev, W. K. Kwok, P. Cheng, L. Fang, and H.-H. Wen, Phys. Rev. B **78**, 140510 (2008).
[66] Z. Pribulova, T. Klein, J. Kacmarcik, C. Marcenat, M. Konczykowski, S. L. Bud'ko, M. Tillman, and P. C. Canfield, Phys. Rev. B **79**, 020508 (2009).
[67] U. Welp, C. Chaparro, A. E. Koshelev, W. K. Kwok, A. Rydh, N. D. Zhigadlo, J. Karpinski, and S. Weyeneth, Phys. Rev. B **83**, 100513 (2011).